Exp.-Nr. **A2**
Eingang:
an PAC:

Mainz Microtron MAMI

A2 Collaboration at MAMI
Spokespersons: P. Pedroni, A. Thomas

Letter of Intent

New Proton Radius Extractions via Precise Measurements of Bethe-Heitler Production

Spokespersons for the Experiment :
Patrik Adlarson, Achim Denig, Michael Ostrick (IKP, Mainz, Germany)
Keith Griffioen (College William and Mary, Williamsburg, USA)
Stanislav Belostotski (Petersburg Nuclear Physics Institute, St. Petersburg, Russia)

Abstract of Physics :
Inconsistent measurements of the proton charge radius constitute one of the most prominent problems in nuclear physics. One explanation involves muons coupling to physics beyond the Standard Model. This letter of intent concerns an experiment suggested by Pauk and Vanderhaeghen (Phys. Rev. Lett. **115** (2015) 221804) to use Bethe-Heitler (BH) production, $\gamma p \to p\ell^+\ell^-$, to test lepton universality. The BH process would also give the possibility to measure the proton radius. For this experiment a high resolution time projection chamber (TPC) with an internal target can be used. We will use a prototype for a test run in 2017, which will serve as a basis for a full proposal in the next run period.

Abstract of Equipment :
The test run will be performed at the tagged photon facility of MAMI with the new Glasgow Tagger. A hydrogen active-target TPC and tracker will measure the recoiling protons and leptons, respectively. A prototype is available in Darmstadt which can be transferred to Mainz. The purpose of the test is to study rates, efficiencies and resolution, in preparation for a full experiment at A2.

MAMI Specifications :

beam energy	1604 MeV
beam polarization	unpolarized

Photon Beam Specifications :

tagged energy range	450 – 1500 MeV
photon beam polarization	unpolarized

Equipment Specifications :

detectors	TPC Prototype from Darmstadt, TAPS, Tagger
target	internal target, Hydrogen, 20 bar

Beam Time Request :

set-up/test with beam	50 hours
data taking	200 hours

1 Physics Motivation

One of the intriguing problems in low energy physics is found in measurements of the charge radius of the proton. Both electrons and muons have been used, and the measured value with muons gives a radius that deviates by 5.6σ compared to measurements with electrons. None of the available explanations for why there is a discrepancy are satisfactory [5, 27].

The proton radius has been measured in both scattering experiments and via atomic spectroscopy. For scattering experiments differential cross sections are measured and the charge radius is extracted from the proton form factors. The charge radius extracted from the elastic electron-proton scattering contains terms dependent on the electric and magnetic form factors, denoted G_E and G_M, respectively. These form factors are studied as function of the electron momentum transfer squared Q^2. The electric and magnetic radii are given by

$$\langle r^2_{E/M} \rangle \equiv -\frac{6\hbar^2}{G_{E/M}(0)} \frac{dG_{E/M}(Q^2)}{dQ^2}|_{Q^2=0}. \quad (1)$$

To extract the proton charge radius the differential cross sections are measured over a range of different momentum transfers, preferably at lower Q^2. The data points are described with a fit function and extrapolated to $Q^2 = 0$. For e-p scattering the most accurate results come from the A1 collaboration [8]. A1 measured over 1400 different data points covering the range in Q^2 from 0.004 to 1 GeV^2. They find $\langle r^2_E \rangle = 0.879(5)_{stat}(6)_{syst}$ fm.

The proton charge radius is also measured from the Lamb shift in hydrogen for transitions between the $2S_{1/2}$ and $2P_{1/2}$ levels [21]. The radius extracted from atomic measurements and scattering measurements are input to the CODATA value of 0.8751(61) fm [27]. The radius has also been extracted with muonic hydrogen. On account of the muon being 200 times heavier than the electron, the muonic wave function overlaps the proton to a much higher degree and is $(200)^3$ times more sensitive to the proton radius. These measurements, made by the CREMA collaboration, obtain the very precise result $\langle r^2_E \rangle = 0.84087(39)$ fm [5, 29]. Compared to the CODATA value, the muonic results deviate by more than 5σ.

Four explanations have been given to explain this surprising discrepancy.

1. The muonic results are wrong. This is being checked with new Lamb shift measurements using muons. The CREMA collaboration will provide energy splittings on other states, such as muonic deuterium and Helium. Recently, the results on the muonic deuterium became public and they find a discrepancy also here, which solidifies the problem [13]. In a few years also muonic scattering data will be available from the MUSE experiment which will measure both $\mu^{\pm}$p and e$^{\pm}$p elastic scattering in the low Q^2, 0.002 to 0.07 GeV^2 [16].

2. There is a problem with the radius extraction for the scattering measurements. Here the discussion revolves around two issues: a) which range in Q^2 is valid for a correct extraction and b) the validity of the fitting function. Based on these evaluations different authors reach different conclusions that favor the muon result, or the A1 results. The spread of values range from $\langle r^2_E \rangle = 0.84(1)$ fm [17, 18, 23, 24] to $\langle r^2_E \rangle = 0.870(26)$ [19] and even $\langle r^2_E \rangle = 0.886(8)$ fm [31]. Even if the scattering data would be compatible with the muonic measurement, the electron

atomic measurements favor the larger radius which then has to find an explanation. PRAD, at Jefferson Lab, which measures G_E at very low Q^2, has taken data and will soon have results.

3. There are QCD corrections that could explain the difference. Two photon effects enter into the theoretical evaluation of the muonic Lamb shift. So far the latest results show that there is some correction but not enough to explain the discrepancy [11].

4. There is an exotic particle involving different couplings to muons and electrons, i.e. physics Beyond the Standard Model (BSM). If this were the case any model involving new physics would have to agree with the constraints of the SM. It would be appealing if one and the same BSM effect could explain both the proton charge radius and the discrepancy currently found between theoretical calculations and measurements of the anomalous magnetic moment of the muon, a_μ. These estimates currently differ by 3–4σ from each other. The problem is that the correction for a_μ is small compared to the effect needed to explain the charge radius discrepancy. There has been work trying to unite these two aspects together. The authors of [12] consider two models - with the new particle either being scalar and pseudo-scalar (S-P) or axial and vector (A-V). The couplings are constrained by a_μ and the muonic Lamb shift, while masses are constrained by kaon decay rate data. They find that S-P masses between 100–200 MeV are ruled out, while for A-V masses below 200 MeV are ruled out. The strength of the coupling for both models approach that of the electromagnetic at ~ 2 GeV. A negative conclusion is instead found by the authors in ref. [6] in which exotic particles are excluded by many low-energy constraints. A third group [32] is more positive to the idea to there being a new exotic particle, favored at the MeV scale.

   Interestingly, in recent years several signs of Beyond Standard Model Physics (**BSM**) have been seen in connection to physics involving leptons. In 2012 the BaBar collaboration reported a 3.4 excess in semi-leptonic B-decay ratios, $\bar{B} \to D^{(*)}\tau\bar{\nu}/\bar{B} \to D^{(*)}l\bar{\nu}$ ($l = e,\ \mu$) compared to the SM [22]. The enhanced rates have since then been confirmed by LHCb (2.1σ) [2], and although Belle agrees with both results and SM [3, 20], when averaging all measurements together the excess becomes 3.9σ [PDG15b]. Another deviation from lepton universality is seen in $B^+ \to K^+l^+l^-$ ($l = e,\ \mu$), with the most precise result finding an excess of 2.6σ compared to SM [1]. As already mentioned a third example is the anomalous magnetic moment of the muon, a_μ, where currently there is a deviation of 3-4σ compared to the SM result [7, 9].

The proton radius puzzle has been around since 2010 and a satisfactory solution will not come from a single experiment that studies the proton radius. Instead, several different approaches are needed. A so far unexplored experimental avenue is the study of the Bethe-Heitler (**BH**) process, $\gamma p \to pl^+l^-$ ($l = e, \mu$), which allows access to the proton form factors and hence also the proton charge radius in a different way. This letter of intent concerns a novel measurement of the proton radius based on this process.

2 Bethe-Heitler

The differential cross-section of the BH process is described by [28]

$$\frac{d\sigma^{BH}}{dtdM_{ll}^2} = \frac{\alpha^3}{(s-M_p^2)^2} \cdot \frac{4\beta}{t^2(M_{ll}^2-t)^4} \cdot \frac{1}{1+\tau} \times \left[C_E G_{E_p}^2 + C_M \tau G_{M_p}^2\right], \tag{2}$$

with t denoting the momentum transfer, M_{ll}^2 the invariant mass squared of the lepton pair, and s the center-of-mass energy squared. $G_{E/M}$ is the proton/magnetic form factor and $C_{E/M}$ are weighting coefficients. The Bethe-Heitler process depends on only three observables and therefore, measuring the beam energy E_γ, the recoiling proton momentum $|p|^{lab}$ and angle θ one can obtain s, t and M_{ll}^2 from the relations

$$s = M_p^2 + 2M_p E_\gamma, \tag{3}$$

$$|p|^{lab} = 2M_p \cdot \sqrt{\tau(1+\tau)},\ \tau = -t/(4M_p^2), \tag{4}$$

and

$$\cos(\theta)_p^{lab} = \frac{M_{ll}^2 + 2(s+M_p^2)\tau}{2(s-M_p^2\sqrt{\tau(1+\tau)}}. \tag{5}$$

Several figures are shown to indicate how the BH cross section depends on each of these respective variables. All three variables play an important role in the BH process and understanding their effects is important for determining the cross section. Differential BH cross sections for the dielectron (solid) and dimuon (dashed) are shown in figure 1 at E_γ=0.5 GeV and E_γ=1.5 GeV. The different colors denote three values of t ranging from the minimum proton momentum which can be measured with the proposed TPC at 20 bar pressure (see next section), $-t = 0.0018$ GeV^2 (p^{lab}=0.042 GeV/c), to the maximum, 0.0420 GeV^2 (0.206 GeV/c).

Figure 2 shows the differential cross section in t for BH-electron as function of p^{lab} (bottom x axis) and $-t$ (top x axis) at three different beam energies. Note the logarithmic scale of both axes. The differential cross section rapidly decreases for increasing proton momenta. Therefore, the lower the proton momentum, the more statistics can be collected. In figure 3 the differential cross section for BH-electron as function of $-t$ and M_{ll}^2 for several different beam energies are shown. The cross section depends primarily on the momentum transfer, although M_{ll}^2 also plays a role. Figure 4 shows the total cross section as function of the beam energy. The di-electron cross-section is $\sim$ 100 mb. Most of these events, however, will be at very low momenta and will not leave a detectable track.

3 Experimental Setup

The experimental setup used for measuring the BH-process is a hydrogen active-target time projection chamber (**TPC**) with a tracker system [33]. The detector is 2 meters long and 1 meter in diameter. The TPC can measure low- to medium- energetic protons with high accuracy and the tracker is used to measure angles of forwardgoing leptons. This TPC is undergoing R&D and is expected to be ready in 2018. For the test beam time described in this LOI a TPC prototype available in Darmstadt will be used [4]. The general idea behind the active target is to use an ionization chamber as an active target

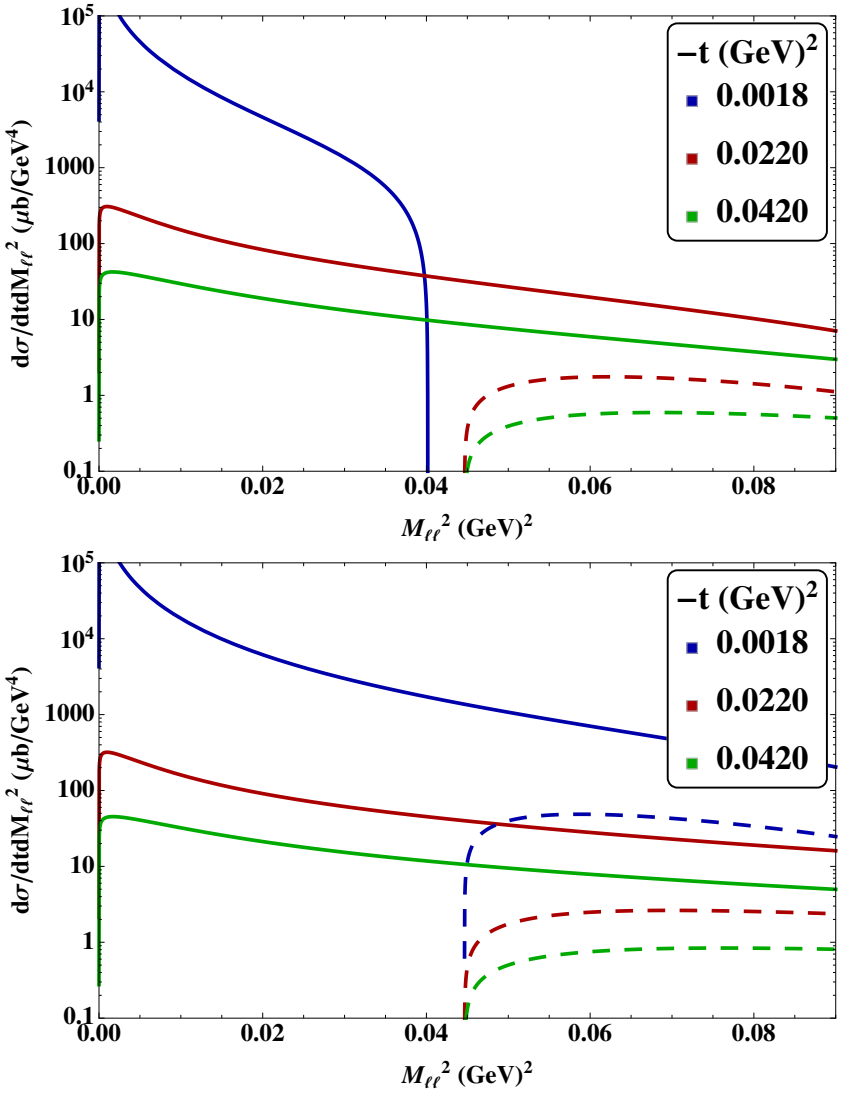

Figure 1: Bethe-Heitler-dielectron (solid) and -dimuon (dashed) differential cross section at different proton momenta produced at the beam energy 0.5 GeV (top) and 1.5 GeV (bottom).

together with the TPC. The advantages are that this avoids wall effects and allows for measuring recoil proton energies even below 1 MeV with an energy resolution of ∼60 keV. With no target container walls a proton efficiency, ϵ, near 100% can be reached [25, 33]. The working gas for the experiment will be H_2 but the possibility exists to also use other gases e.g. D_2, He_3, He_4 or CH_4. More detailed information on the prototype and final TPC layout is found in LOI2016-2.

3.1 Focal Plane Detector

Common to both the test-time and final setups is that the upgraded Focal Plane Detector (**FPD, tagger**) of the A2 tagging spectrometer will be used [26, 30]. The benefits of the new tagger is that higher rates are possible compared to the existing system. Given the relatively low BH dimuon cross section, a high luminosity is needed to reach adequate

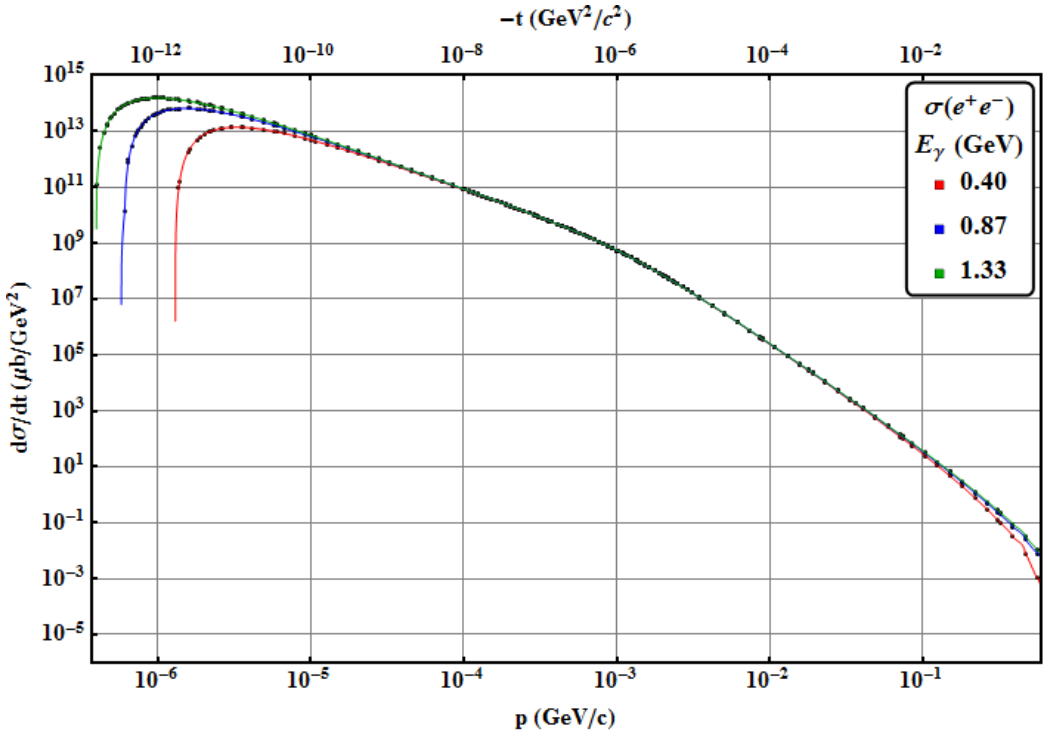

Figure 2: BH-dielectron differential cross section as function of proton momentum/momentum transfers for three beam energies.

statistics in a reasonable amount of time. The luminosity may be increased either from a high photon flux and/or from an increased target density. The maximum photon beam flux is evaluated as the maximum electron rate that any one focal plane detector element can handle before reaching saturation. Since the bremsstrahlung density profile goes as $1/E_\gamma$, the maximum rate is given by the tagger element which corresponds to the lowest photon energy, f_{min}. The current FPD elements can handle rates of approximately 1 MHz, while the new tagger will increase this by a factor of 5. A factor of 2 is gained from using more non-overlapping scintillator elements while another factor of 2.5 comes from installing silicon PMTs and new electronics. It may still turn out that a fivefold increase is not practically achievable. One caveat is that the effective maximum depends on both prompt hits and random hits. Another limiting factor may be the online DAQ. For these reasons one of the tests that will be performed is to measure the maximum photon flux which can be obtained. As seen in figure 4 the BH-dimuon cross-section increases as a function of beam energy. To maximize the number of dimuon events the (unpolarized) beam should be set to the highest possible energy provided by MAMI-C, which is 1604 MeV.

3.2 Final Setup

The proposed TPC is an upgraded version of the proton recoil detection apparatus IKAR. IKAR has previously been used in the CERN's WA9 and NA8 experiments for measuring small-angle pp and πp scattering [10, 33] and subsequently also for nuclear-matter distributions in neutron-rich Li isotopes at GSI [14]. The same setup will also be used in LOI2016-2- "High Precision Measurement of the ep-elastic cross section at small Q2".

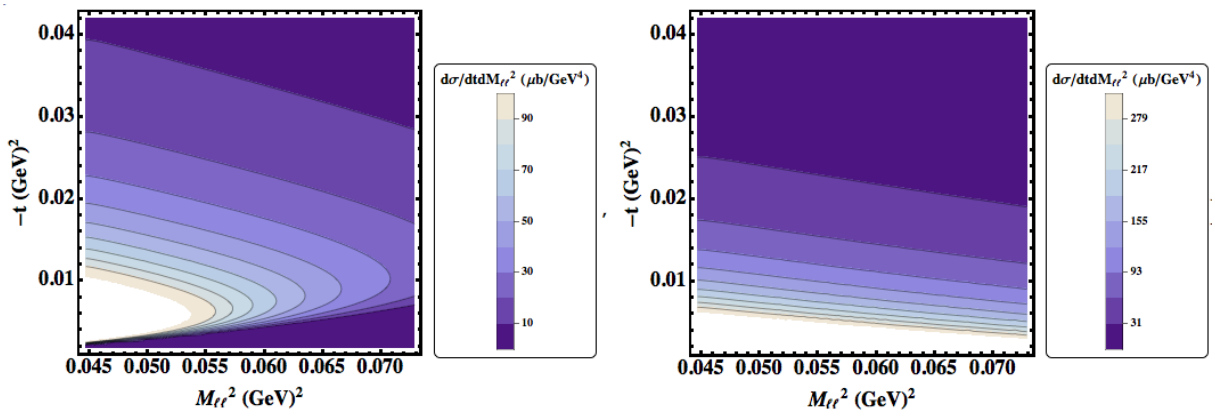

Figure 3: BH-dielectron differential cross section as function of momentum transfer (y-axis) and invariant mass squared of the dileptons (x-axis) at E_γ=0.5(1.5) GeV left(right).

Gas	H_2, D_2, He_3, He_4, CH_4
Gas pressure (bar)	4, 20
Drift distance, (mm)	300± 0.1
σ_z (μm)	150
σ_{T_p} (keV)	60
σ_{θ_p} (mrad)	10-15
$\sigma_{x/y/z}$ tracker (z TPC) (μm)	30/30/150
σ_t TPC/ tracker (ns)	40/5
θ_{max} (°)	32

Table 1: TPC and tracker specifications.

Drawings of the detector setup are shown in figures 5 and 6. The proposed TPC will be able to measure the recoil proton and the forward-scattered leptons. The active gas, H_2 will be mainly operated at 20 bars, corresponding to a proton target thickness of $3.6{\cdot}10^{22}$ p/cm^2. Under these pressures proton kinetic energies from roughly 1–20 MeV can be measured. This corresponds to -t = 0.002 - 0.04 GeV^2. Lower pressures may also be used to accurately probe the low energy region. The projected specifications of the detector are shown in table 1.

3.3 Test Setup

For the test beam time a TPC prototype will be used. It was originally constructed as an ACTAR2 prototype for the R3B experiment at FAIR, GSI [4]. The use of that setup was for a test experiment with a 700 MeV/u ^{58}Ni beam. The prototype is similar to the TPC proposed in the final setup, although it is smaller and operates with lower gas pressures (10 bar). An important difference compared to the final setup is the absence of a tracker in the test prototype which will affect the triggering. To reduce the DAQ rates one cannot trigger on the recoil protons alone. Additionally, the timing signal of the TPC is relatively slow. For fast triggering one has to trigger on at least one of the BH leptons. In the final setup the timing resolution is expected to be in the order of a few ns (compared to the TPC $\sim$ 40 ns). TAPS will be integrated into the setup in order to be

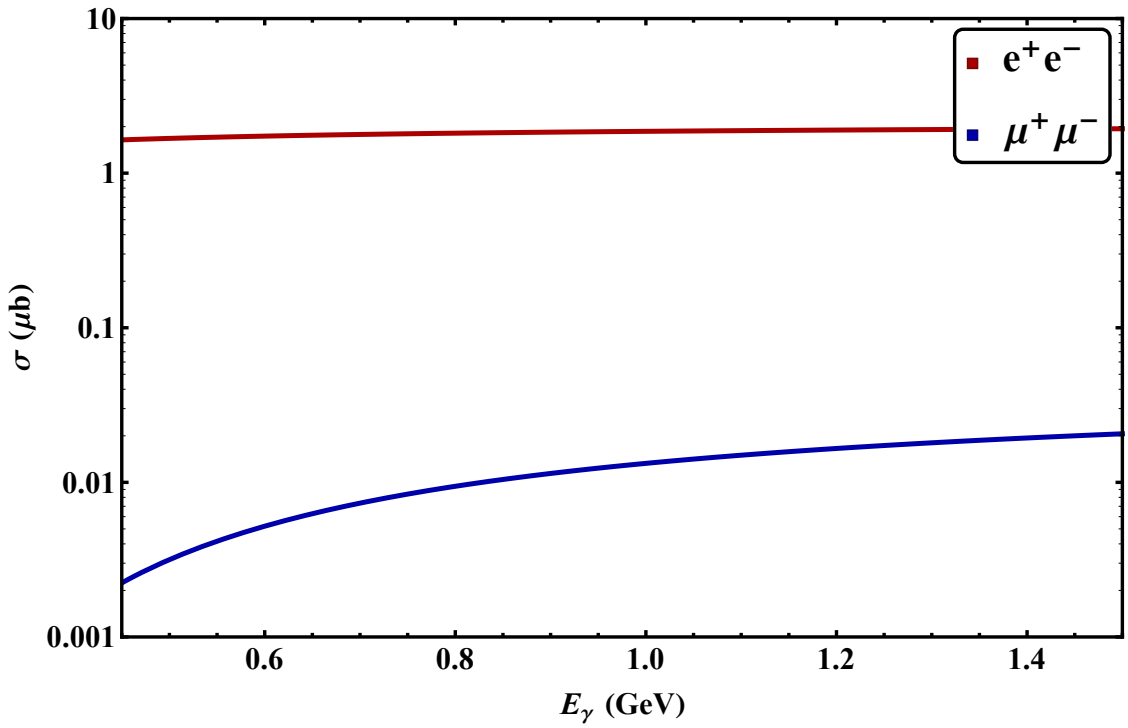

Figure 4: BH-dielectron (red) and BH-dimuon (blue) total cross section as function of beam energy.

able to trigger on the BH process during the test beam time. An event will be triggered based on a multiplicity of two in TAPS with a fast-clear if there is no signal in the active target region. If successful TAPS may also be included as part of the final setup.

A schematic view of ACTAR2 is shown in figure 7. The TPC system, the cathode, anodes and grid are inside a cylindrical aluminum volume, 0.60 m long and internal diameter of 0.29 m. The anode electrodes are divided into 66 different segments, each of which read-out independently with the energy resolution of $\sigma_E \sim 20$ keV.

4 Rate Calculation

The BH differential cross section of Eq. 2 is first integrated over the desired range in $M_{\ell\ell}^2$ and t. Generally, invariant square masses between dielectron threshold (1.04×10^{-6} GeV^2) and di-neutral pion threshold (0.073 GeV^2) and $-t$ values in the range of the TPC detector (0.0018 to 0.0420 GeV^2) are considered. These integrals are performed numerically and produce a differential cross section that is a function of E_γ like those shown in Figure 4.

The goal for the new tagger is to have a maximum photon rate flux per channel of 5 MHz. The bremsstrahlung dependence follows a $1/E_\gamma$ distribution so the overall photon rate flux should be normalized by some constant C, that sets the lowest focal plane detector to 5 MHz,

$$5\times10^6 = C\int_{E_{min}}^{E_{max}} \frac{1}{E_\gamma} dE_\gamma. \tag{6}$$

The total photon flux is then the cross section multiplied by the bremsstrahlung distribution over the full range of the photon energies. For the case where the photon energy

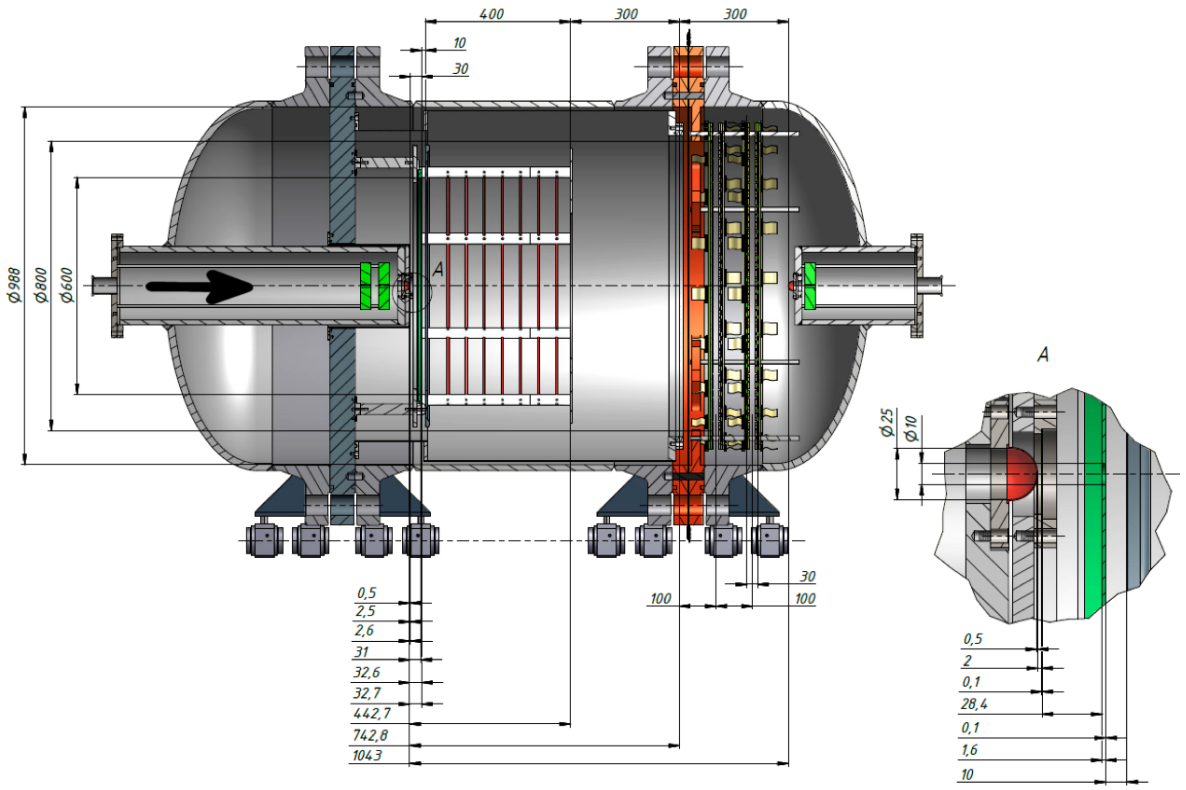

Figure 5: Drawing of TPC and tracker system projected to be used in the final setup. Beam photons enter from left (in direction of arrow), through the 0.5 mm Beryllium window (see A for zoom-in), where it interacts with the active gas. A Mylar membrane separates the tracking- from the TPC-volume. Figure from LOI2016-2.

range extends from 0.45 to 1.50 GeV there is an expected rate of $\Phi = 3.8 \times 10^8$ Hz. Finally, the TPC is 35 cm long and will operate at 20 bars- this corresponds to a proton target thickness of approximately 3.6×10^{22} nucleons/cm^2. For the tagging efficiency 70% has been assumed, estimated from fig 4.32 in [34]. The tagged luminosity is therefore approximately $1 \times 10^{31}\ cm^{-2}s^{-1}$ *†.

The BH differential cross section at this point is a function of E_γ, so the luminosity is written as a function of E_γ as well by normalizing it such that the total luminosity is $L_{tot} \sim 1 \times 10^{31}\ cm^{-2}s^{-1}$,

$$L(E_\gamma) = \frac{L_{tot}}{\log\left(E_{max}/E_{min}\right)} \frac{1}{E_\gamma}. \tag{7}$$

The total cross section is found by integrating,

$$\sigma_{tot} = \int_{E_{min}}^{E_{max}} \sigma(E_\gamma) L(E_\gamma) dE_\gamma. \tag{8}$$

*It is perhaps important to make a distinction here. The luminosity calculated here is the tagged luminosity, which means the luminosity for which the bremsstrahlung electrons are within the kinematical range of the tagger. The total luminosity is of course higher.

†A 70% tagging efficiency gives $1.2 \times 10^{31}\ cm^{-2}s^{-1}$. If a 40% tagging efficiency is assumed, the corresponding tagged luminosity would be $6.9 \times 10^{30}\ cm^{-2}s^{-1}$

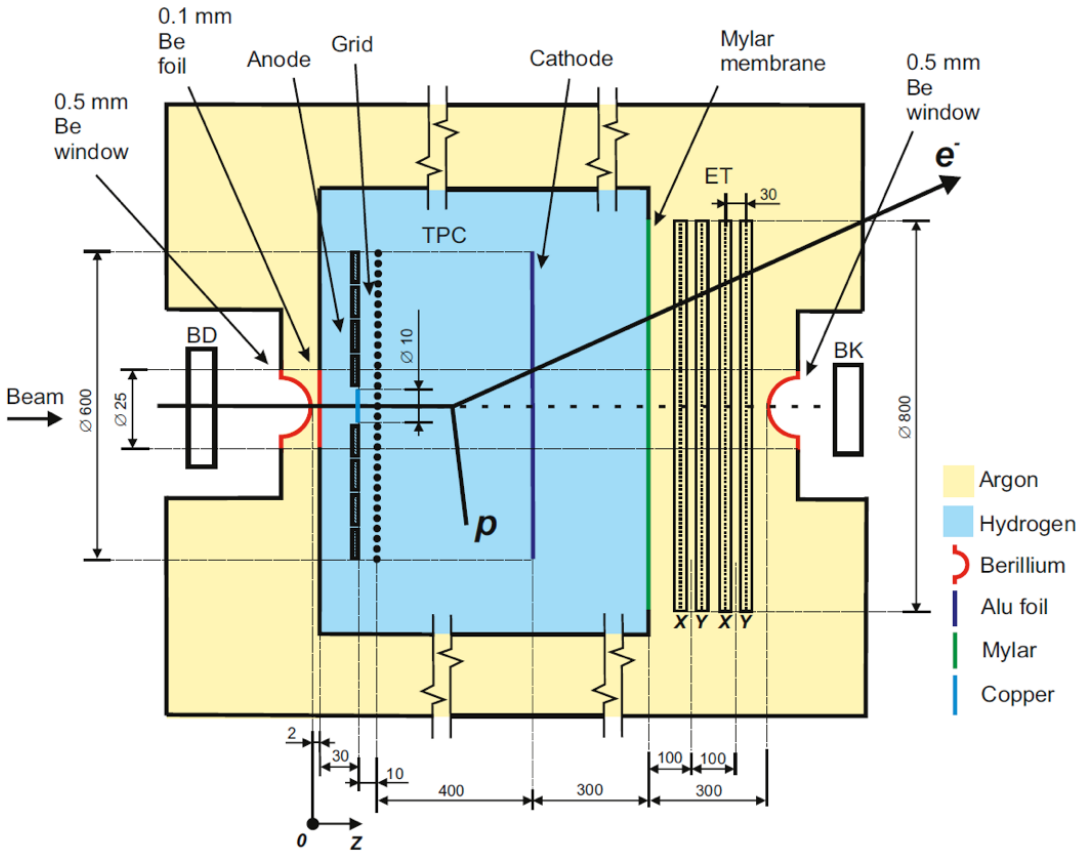

Figure 6: Schematic diagram of the detector system as envisaged for ep-scattering. The beam particle enters from left through the Beryllium window and interacts with the active H_2 gas. The recoil proton energy and theta angles are measured as the forward-scattered electrons are tracked in the four wire planes. Figure from LOI2016-2.

The dielectron production rate is much larger than the dimuon rate (c.f. figure 4). Similarly, the dielectron rate below dimuon threshold is much larger than that of the dilepton rate above dimuon threshold. This is because of the limited background free space below dipion threshold. The effects of this discrepancy is discussed in section 5. The expected rates of the $\gamma p \to p\ell^+\ell^-$ process are listed in Table 2. These statistics are preliminary estimates based on the assumed specifications of the final TPC and as such are subject to change.

	$M^2_{\ell\ell} \leq 4m^2_\mu$	$e^+e^-, 4m^2_\mu < M^2_{\ell\ell} < 4m^2_{\pi_0}$	$\mu^+\mu^-, 4m^2_\mu < M^2_{\ell\ell} < 4m^2_{\pi_0}$
$\approx$ Event Rate (Hz)	21	1.05	0.07
$\approx$ Events (30 Days)	6.09×10^7	2.60×10^6	1.40×10^5

Table 2: Event rates and expected events for dilepton processes below and above dimuon threshold based on assumed luminosity and without considering systematic effects.

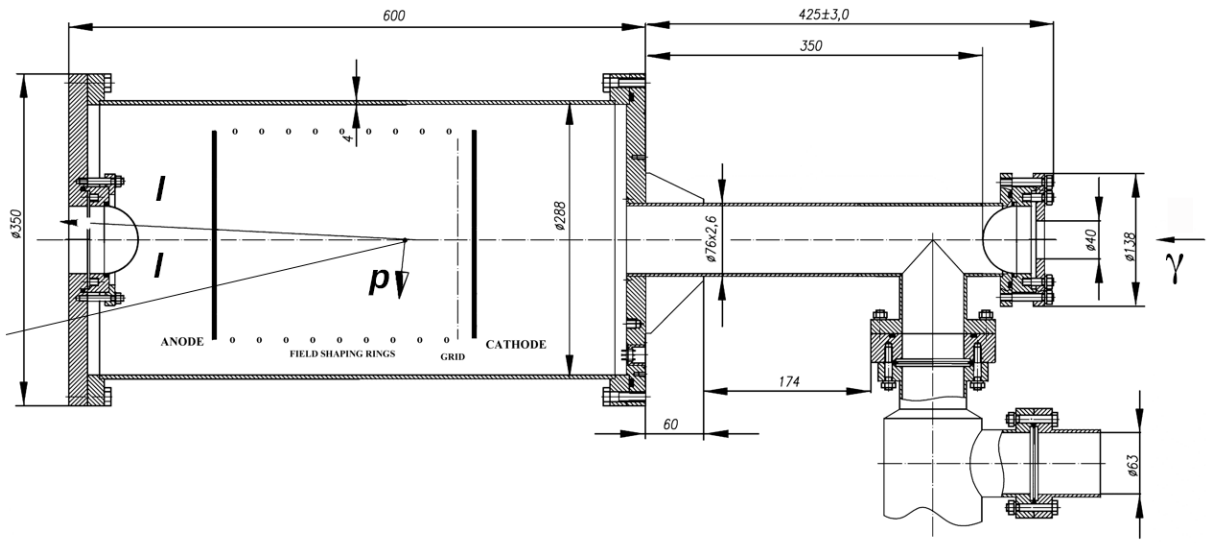

Figure 7: Schematic view of the ACTAR2 prototype setup to be used in the test beam time. In the figure the beam photon enters from the right and interacts with the active gas, which produces the BH reaction.

5 Analysis

There are three ways used for investigating the BH data: a comparison of cross section rates above and below muon threshold in order to test lepton universality, an extraction of the proton radius via the pure dielectron signal below muon threshold and an overall test of the BH differential cross sections. These methods are similar in their execution and in many ways depend on each other and so will be explained in unison. Some additional steps will be required because we rely on extracting information from the BH via ratios of cross sections.

The method described by Pauk and Vanderhaegen relies on the ratio of differential cross sections below and above muon threshold at certain fixed values of t and E_γ where an effect of lepton universality is most clearly seen [28]. The ratio is given by

$$R_{\mu/e} = \frac{d\sigma(e^+e^- + \mu^+\mu^-)}{d\sigma(e^+e^-)} - 1. \tag{9}$$

Unfortunately, the restriction to fixed values of two out of the three variables severely limits the statistics. If instead the total BH cross section (i.e. all detectable $M^2_{\ell\ell}$, t and E_γ values) is used then the possibility exists to make a test of lepton universality using all data. The example provided in the paper, seen on the top in figure 8 shows a 0.2% effect in the ratio at $E_\gamma = 0.5$ GeV and $-t$=0.03 assuming G^e_E/G^μ_E=1.01. The form factor is, however, dependent on $-t$ as shown on the bottom in figure 8 and so the difference in ratios will depend on the proton transfer momenta range. The slope of the line would change from new physics because the Bethe-Heitler process couples differently to muons and electrons. The higher the momentum transfer, the bigger the difference in form factors (but also the smaller the cross section).

Below muon threshold it is possible to make a measurement of the proton radius by dividing the pure dielectron signal into two regions and comparing their total cross

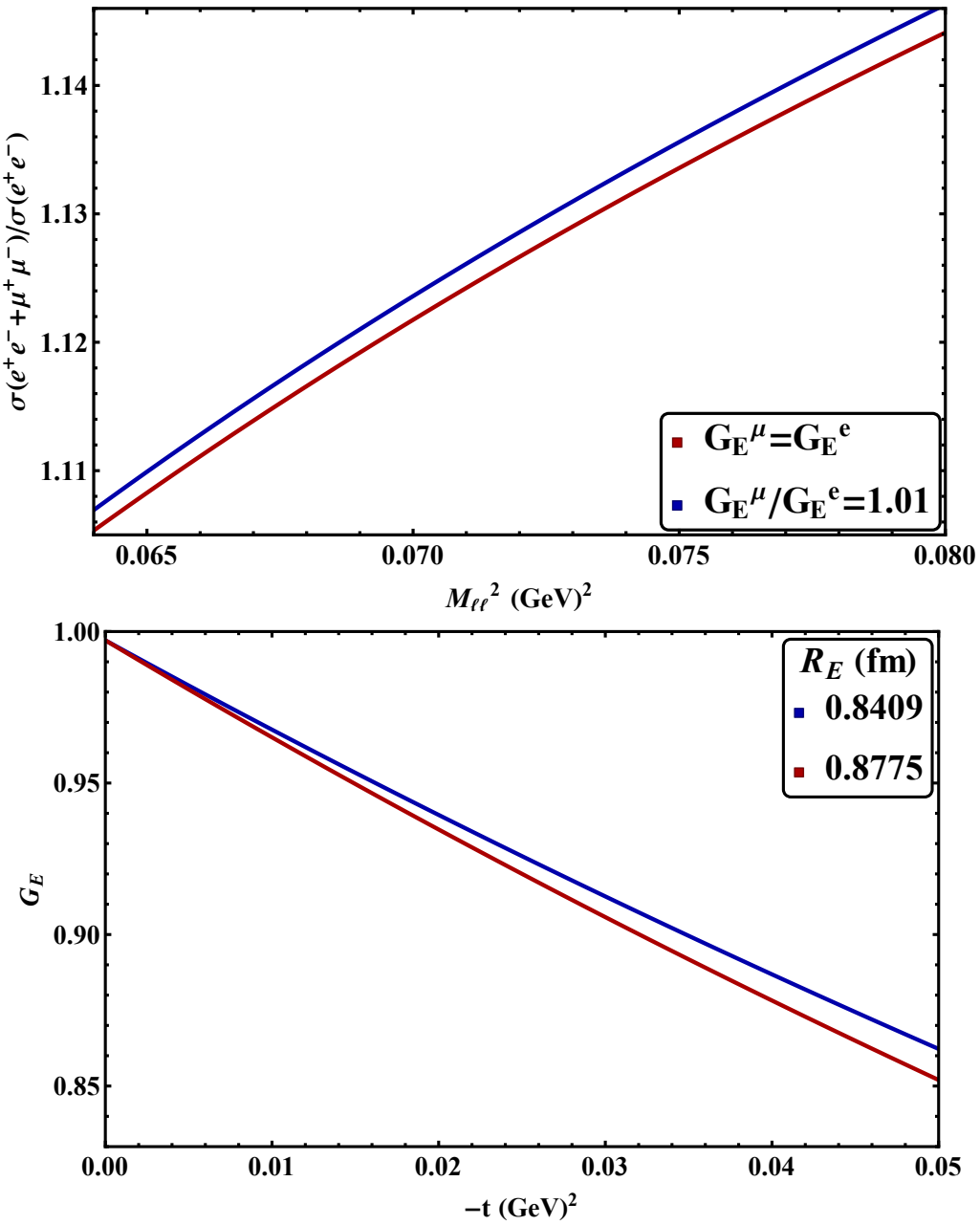

Figure 8: $R_{\mu/e}$ for $-t = 0.03$ GeV^2 and $E_\gamma = 0.5$ GeV for the case of lepton universality and a 1% difference in the electron and muonic form factors (top) and G_E as a function of $-t$ for the two cases of proton radii (bottom).

section. In figure 9 the ratio of cross sections in the regions $M_{\ell\ell}^2 = [4m_e^2, 0.4 \times 4m_\mu^2]$ and $M_{\ell\ell}^2 = [0.4 \times 4m_\mu^2, 4m_\mu^2]$ are shown. Given the expected statistics discussed in section 4 and assuming perfect detection efficiency, it should be possible to clearly distinguish between the CODATA result (0.8775 fm) and the muonic lamb shift result (0.8409 fm). Again, these statistics (and all subsequent statistics) are based on assumptions of the final TPC and are subject to change. This particular choice of regions is in a sense arbitrary and the expected statistics should be consistent regardless of what regions are used.

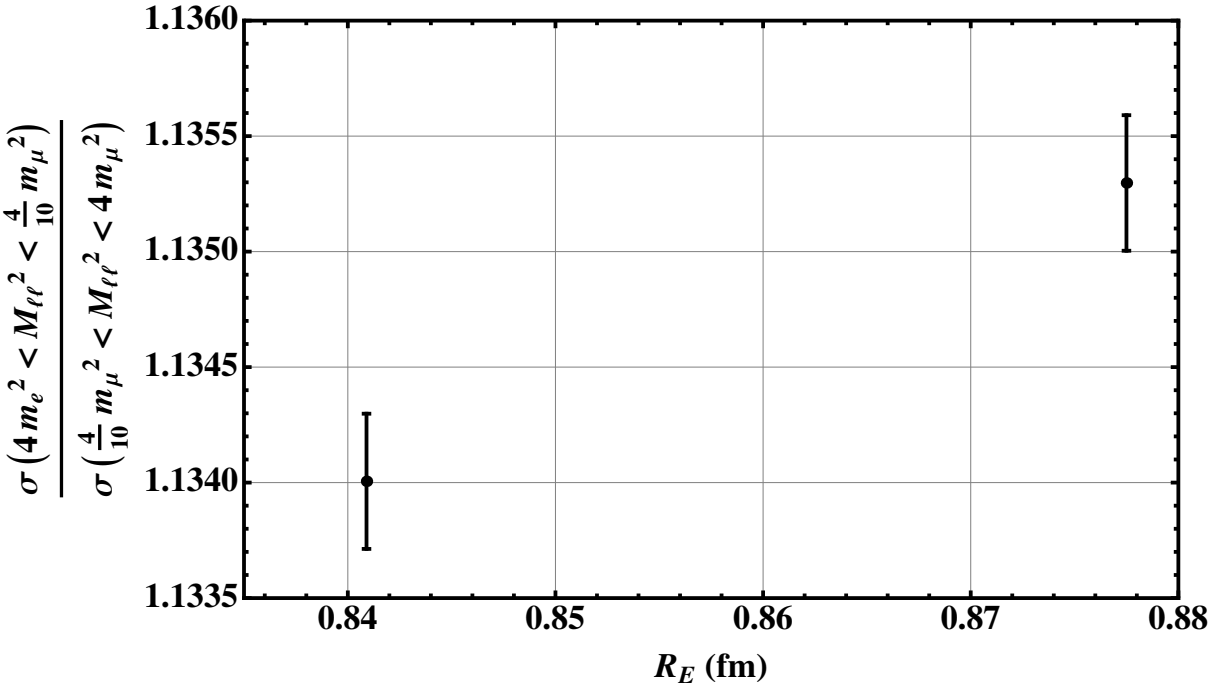

Figure 9: Extracted ratio of dielectron cross section between two arbitrary regions below dimuon threshold for different values of the proton radius. The error bars are based on the TPC specifications discussed in section 4.

Once a proton radius has been established from the pure electron signal below the dimuon threshold it is possible to test lepton universality by looking at a signal that includes BH-dimuons. With the proposed setup one will not be able to discern between electrons and muons and so will have to rely on the mixed signal of leptons above the dimuon threshold. There is only one correct proton radius, but if there is new physics that breaks lepton universality one will interpret the effects of this new "BH-like" process as corresponding to a different proton radius for the muonic case. This should alter the measured cross section away from the expected value for the case where both radii are the same. In figure 10 this possibility is investigated. It will however be difficult to make a statistically significant differentiation between the two possibilities given just 30 days of beam time.

In addition the BH data can be used to extract the electric form factor. At low transfer momentum the proton radius can be determined from the coefficient of the linear term, c_1, of a fit via,

$$c_1 = \frac{1}{6}\left(\frac{R_E}{\hbar c}\right)^2. \tag{10}$$

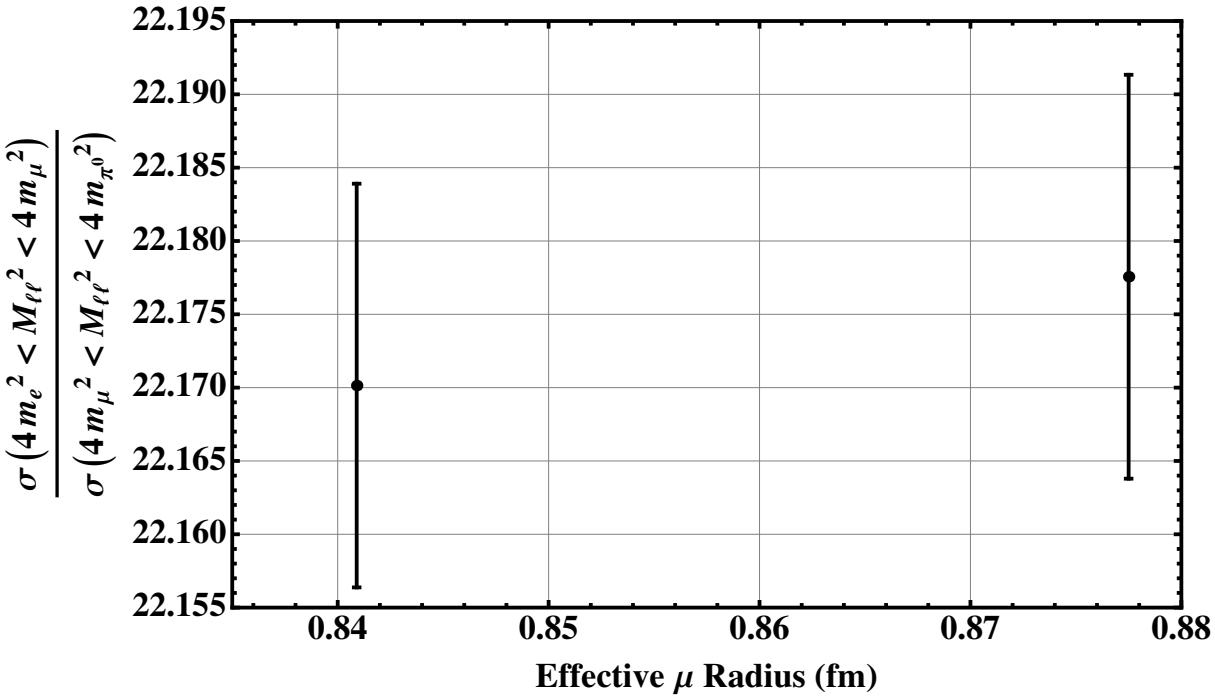

Figure 10: Extracted ratio of dielectron cross section below dimuon threshold and dilepton production above dimuon threshold (a cut is applied at dipion threshold). The effective electronic-proton radius is assumed to be the CODATA value, 0.8775 fm [27] and points are shown for both cases for the effective muonic-proton radius. The error bars are based on the TPC measuring the proton in the -t range 0.002-0.042 GeV^2 and 100% efficiency, as discussed in section 4.

Figure 11 shows a possible measurement of the proton radius measured in this experiment. The range in detectable t values has been divided up into 50 bins and the statistics is calculated for each bin assuming the rates discussed in Section 4 and 30 days of beam time. The data points have been smeared with σ equal to the statistical uncertainty of each corresponding bin. The statistics adjusted data has then been fit to a linear function and the proton radius extracted from the slope. There will, of course, be systematics to deal with but a sub-1% uncertainty should be possible and a statistically significant difference should be visible to discern between the CODATA [27] and muonic lamb shift results. The extraction of the proton charge radius will be done using a relative measurement. This is the same strategy as adopted by e.g. the MUSE collaboration [15].

Finally, one will be able to use the experimental data to test the theoretical predictions by comparing the BH differential cross sections as function of s, t and $M^2_{\ell\ell}$.

6 Background

Possible sources of background which can mimic the BH-process have also been considered. These processes are time-like virtual Compton scattering, Compton scattering, direct π^0 production, and the direct $\pi^+\pi^-$ production. Common to these reactions is that the proton phase space for the background are close or partially overlap with the BH-

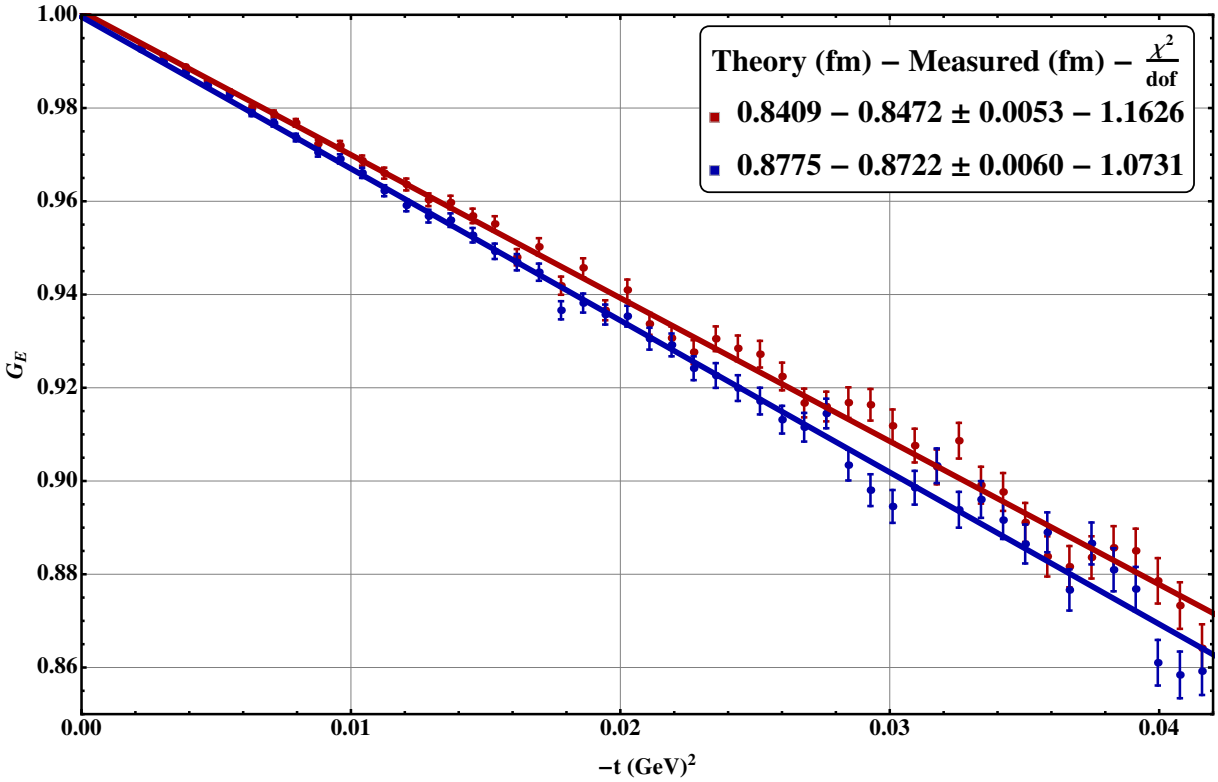

Figure 11: Possible experimental measurement of G_E for the case where $R_E = 0.8409$ fm and 0.8775 fm. The error bars are based on the TPC specifications discussed in section 4.

associated proton. Another common feature is that the final state particles involve two charged tracks.

The time-like virtual Compton scattering has an identical final-state topology and its contribution has to be estimated. The effect of this process has been considered in a one paragraph discussion in Pauk-Vanderhaeghen [28]. They estimate the effect from the timelike Compton Born contribution and find it to be roughly a factor of 5 smaller than G_E^μ/G_E^e=1% and further comment that $R_{\mu/e}$ is not very sensitive to possible previous inaccuracies in the study of the time-like Compton prospect.

The Compton scattering with a real photon can via conversion produce an e^+e^- pair. The neutral single-pion production could mimic the signal process if one of the decaying photons convert into an e^+e^- pair, or from its Dalitz decay branching ratio, BR($\pi^0 \to e^+e^-\gamma$) = 1.17%. If the vertex resolution is precise enough, a secondary vertex could be identified and distinguished from the production vertex. Thus these conversion events could possibly be removed for many cases.

A second way to constrain the Compton scattering background is to use equation (3) to calculate M_{ll}^2 and remove this contribution by a cut. This strategy can also be applied for the other background processes. Alternatively, a cut can be made on the proton energy versus angle in the regions of phase space with background reactions present. An example of the proton momentum versus its polar angle phase space is shown for the di-electron and di-muon in the top and bottom frame of figure 12, respectively. The signal processes are shown in color while the recoil proton for (on-shell) Compton scattering,

direct π^0 and direct $\pi^0\pi^0$ production are shown in black. The background process which is most serious to the BH-dimuon is the charged dipion production, $\gamma p \to \pi^+\pi^- p$. It has a much larger cross-section and since pions and muons are relatively close to each other in mass, the phase space of these two reactions to a large degree overlap. Also, due to the detector resolution, there is not a sharp edge with which to separate the dipion from the BH-phase space. To determine the proton energy and angular resolution is therefore another important aspect which a test beam time could help determine.

7 Beam Time request

Two weeks of beam time are asked for. There are a few fundamental questions that this test beam time is expected to answer. What rates can be effectively reached in the final version of the experiment? The answer to this question is connected to the interplay between the beam intensity, the performance of the upgraded tagger, the online Data Acquisition System and how effective the trigger is. What is the proton energy and angular resolution that can be achieved? Which proton energy range can be probed by the TPC. These two variables are related to the proton energy range that can be measured. A lower pressure decreases the maximum proton energy which can be measured. On the other hand this would allow for a better resolution. If one instead uses CH_4, operated under 20 bars, one can increase t_{max} by a factor of 2. CH_4 could however give problems from quasi-elastic proton scattering. A test beam time could indicate the viability of using another gas. A third is the effect of background reactions may have, especially from charged two-pion production. The experimental setup is completely new to the A2 hall so much experience will be gained from answering these and other questions. These answers may also provide the answers at an early stage what systematical effects which are important.

Ideally, the outcome of the test beam time is that one will be able to reconstruct the Bethe-Heitler dielectron and produce experimental numbers for resolution, effective rates and signal-to-background. To do this, the active target has to be integrated to the A2 DAQ system together with the TAPS detector.

Another motivation for doing a test run is to look at the active target in a long term perspective. If successful, one can envision that the experimental setup also could be used to study a number of other different physics processes, including e.g., Bethe-Heitler explorations of deuterium.

References

[1] Roel Aaij et al. Test of lepton universality using $B^+ \to K^+\ell^+\ell^-$ decays. *Phys. Rev. Lett.*, 113:151601, 2014.

[2] Roel Aaij et al. Measurement of the ratio of branching fractions $\mathcal{B}(\bar{B}^0 \to D^{*+}\tau^-\bar{\nu}_\tau)/\mathcal{B}(\bar{B}^0 \to D^{*+}\mu^-\bar{\nu}_\mu)$. *Phys. Rev. Lett.*, 115(11):111803, 2015. [Addendum: Phys. Rev. Lett.115,no.15,159901(2015)].

[3] A. Abdesselam et al. Measurement of the branching ratio of $\bar{B}^0 \to D^{*+}\tau^-\bar{\nu}_\tau$ relative to $\bar{B}^0 \to D^{*+}\ell^-\bar{\nu}_\ell$ decays with a semileptonic tagging method. 2016.

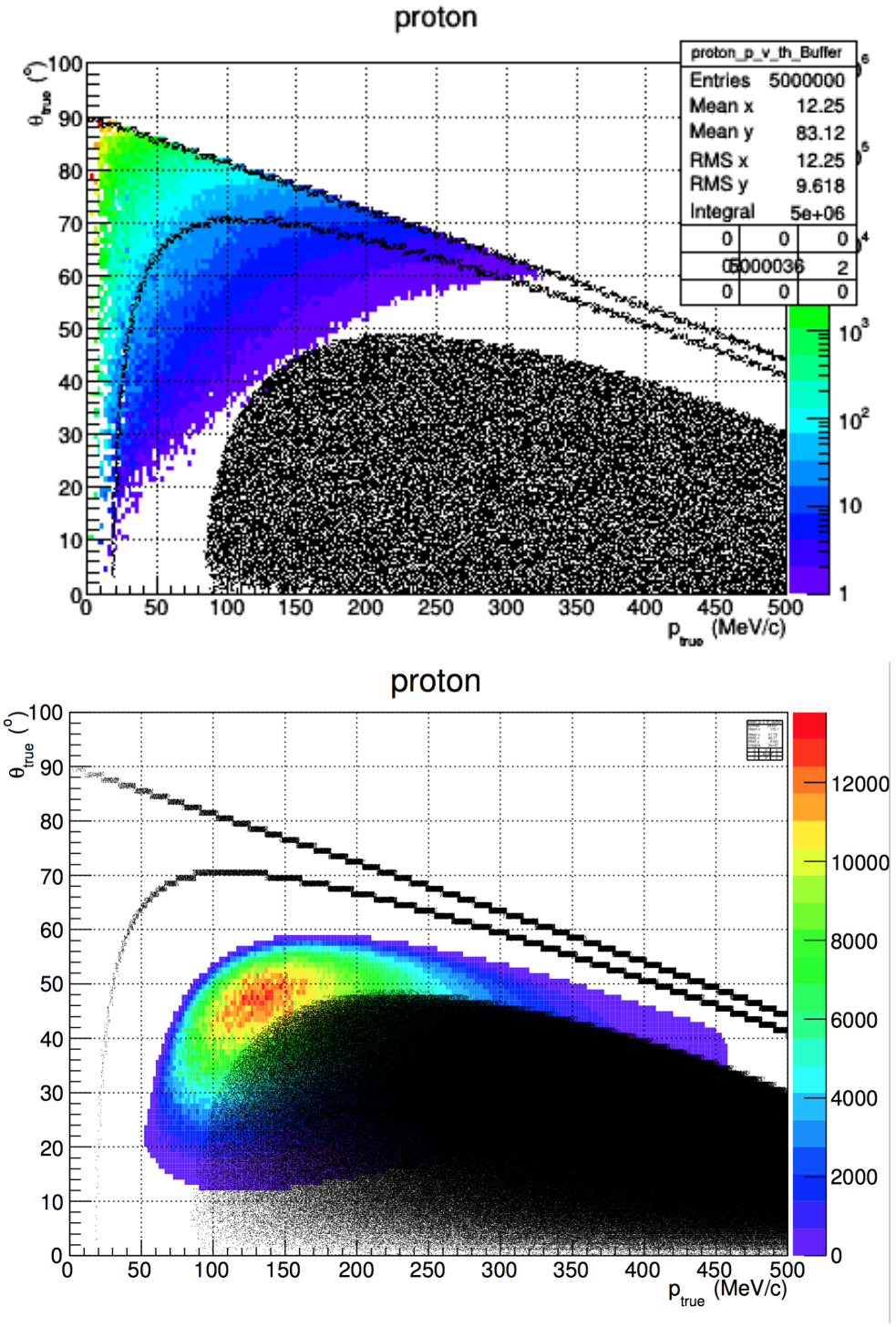

Figure 12: BH-dielectron (top) and BH-dimuon (bottom) true proton momenta versus theta with three background processes in black. Simulated at the beam energy 0.5 GeV.

[4] G. Alkhazov. Test of an r3b active target prototype with a beam of 58ni. *GSI Scientific Report 2014*, https://repository.gsi.de/record/183651/files/SR2014-Part-NUSTAR.pdf:191, 2015.

[5] Aldo Antognini et al. Proton Structure from the Measurement of $2S-2P$ Transition Frequencies of Muonic Hydrogen. *Science*, 339:417–420, 2013.

[6] Vernon Barger, Cheng-Wei Chiang, Wai-Yee Keung, and Danny Marfatia. Proton size anomaly. *Phys. Rev. Lett.*, 106:153001, 2011.

[7] G. W. Bennett et al. Final Report of the Muon E821 Anomalous Magnetic Moment Measurement at BNL. *Phys. Rev.*, D73:072003, 2006.

[8] J. C. Bernauer et al. High-precision determination of the electric and magnetic form factors of the proton. *Phys. Rev. Lett.*, 105:242001, 2010.

[9] Thomas Blum, Achim Denig, Ivan Logashenko, Eduardo de Rafael, B. Lee Roberts, Thomas Teubner, and Graziano Venanzoni. The Muon (g-2) Theory Value: Present and Future. 2013.

[10] J. P. Burq et al. Soft $\pi^- p$ and pp Elastic Scattering in the Energy Range 30-GeV to 345-GeV. *Nucl. Phys.*, B217:285–335, 1983.

[11] Carl E. Carlson. The Proton Radius Puzzle. *Prog. Part. Nucl. Phys.*, 82:59–77, 2015.

[12] Carl E. Carlson and Benjamin C. Rislow. New Physics and the Proton Radius Problem. *Phys. Rev.*, D86:035013, 2012.

[13] Randolf Pohl et al. CREMA collaboration. Laser spectroscopy of muonic deuterium. *Science*, 353(6300):669, August 2016.

[14] A. V. Dobrovolsky et al. Study of the nuclear matter distribution in neutron-rich Li isotopes. *Nucl. Phys.*, A766:1–24, 2006.

[15] R. Gilman et al. A proposal for the paul scherrer institute m1 beam line studying the proton radius puzzle with p elastic scattering the muon proton scattering experiment (muse) collaboration. *http://www.physics.rutgers.edu/~rgilman/elasticmup/muse_prop_2012.pdf*, 2012.

[16] Ronald (MUSE Collaboration) Gilman et al. Studying the proton "radius" puzzle with μp elastic scattering. *arXiv:1303.2160*.

[17] Keith Griffioen, Carl Carlson, and Sarah Maddox. Consistency of electron scattering data with a small proton radius. *Phys. Rev.*, C93(6):065207, 2016.

[18] Douglas W. Higinbotham, Al Amin Kabir, Vincent Lin, David Meekins, Blaine Norum, and Brad Sawatzky. Proton radius from electron scattering data. *Phys. Rev.*, C93(5):055207, 2016.

[19] Richard J. Hill and Gil Paz. Model independent extraction of the proton charge radius from electron scattering. *Phys. Rev.*, D82:113005, 2010.

[20] M. Huschle et al. Measurement of the branching ratio of $\bar{B} \to D^{(*)}\tau^-\bar{\nu}_\tau$ relative to $\bar{B} \to D^{(*)}\ell^-\bar{\nu}_\ell$ decays with hadronic tagging at Belle. *Phys. Rev.*, D92(7):072014, 2015.

[21] Willis E. Lamb and Robert C. Retherford. Fine Structure of the Hydrogen Atom by a Microwave Method. *Phys. Rev.*, 72:241–243, 1947.

[22] J. P. Lees et al. Evidence for an excess of $\bar{B} \to D^{(*)}\tau^-\bar{\nu}_\tau$ decays. *Phys. Rev. Lett.*, 109:101802, 2012.

[23] I. T. Lorenz, H. W. Hammer, and Ulf-G. Meissner. The size of the proton - closing in on the radius puzzle. *Eur. Phys. J.*, A48:151, 2012.

[24] I. T. Lorenz and Ulf-G. Meißner. Reduction of the proton radius discrepancy by 3σ. *Phys. Lett.*, B737:57–59, 2014.

[25] Evgeny Maev. New experimental method for investigation of the nucleon polarizabilities t mesa. In *https://indico.mitp.uni-mainz.de/event/66/*, 2016.

[26] J. C. McGeorge et al. Upgrade of the Glasgow photon tagging spectrometer for Mainz MAMI-C. *Eur. Phys. J.*, A37:129–137, 2008.

[27] Peter J. Mohr, David B. Newell, and Barry N. Taylor. CODATA Recommended Values of the Fundamental Physical Constants: 2014 - Summary, August 2015.

[28] Vladyslav Pauk and Marc Vanderhaeghen. Lepton universality test in the photoproduction of e^-e^+ versus $\mu^-\mu^+$ pairs on a proton target. *Phys. Rev. Lett.*, 115(22):221804, 2015.

[29] Randolf Pohl et al. The size of the proton. *Nature*, 466:213–216, 2010.

[30] A. Reiter et al. *Eur. Phys. J.*, A 30:461, 2006.

[31] Ingo Sick. Problems with proton radii. *Prog. Part. Nucl. Phys.*, 67:473–478, 2012.

[32] David Tucker-Smith and Itay Yavin. Muonic hydrogen and MeV forces. *Phys. Rev.*, D83:101702, 2011.

[33] A.A. VOROBYOV. Proposal for high precision measuremens of the e-p differential cross section at small t-values with the recoiled proton detector. In *https://indico.mitp.uni-mainz.de/event/66/*, 2016.

[34] Dominik Werthmueller. *Experimental study of nucleon resonance contributions to eta photoproduction on the neutron*. PhD thesis, Universität Basel, 2014.